Shear strengths of joints with roughened concrete surfaces and post-installed dowel bars subjected to normal and shear stresses for seismically retrofitted structures

メタデータ	言語: English 出版者: Elsevier 公開日: 2023-12-21 キーワード (Ja): キーワード (En): Roughened concrete surface, Bearing failure, Dowel action, Seismic retrofit, Combined stress 作成者: 髙瀬, 裕也, Yamada, Taizo メールアドレス: 所属:
URL	http://hdl.handle.net/10258/0002000162

Shear strengths of joints with roughened concrete surfaces and post-installed dowel bars subjected to normal and shear stresses for seismically retrofitted structures

Yuya Takase*
Associate Professor, College of Design and Manufacturing Technology, Muroran Institute of Technology, Japan y.takase@mmm.muroran-it.ac.jp

Taizo Yamada
Graduate Student, College of Environmental Technology, Muroran Institute of Technology, Japan

ABSTRACT: When reinforced concrete (RC) structures are seismically retrofitted, new members are connected via joints with roughened surfaces and post-installed dowel bars. For retrofitted RC buildings, roughened surfaces are often manufactured using vibration hammers. However, investigations on the shear strengths of the joints subjected to shear and tensile normal stresses are limited. In this study, these joints, called hybrid joints, were subjected to shear loading. The test parameters were the normal stress, dowel bar diameter d_d, and roughened concrete area ratio r_{rc}. The normal stress was set to have a compressive stress σ_0 of –0.48 N/mm^2 and a ratios r_N of tensile stress to yield strength of 0.00, 0.33, and 0.66. In addition, dowel bars with d_d = 13, 16, and 19 mm were used. The target r_{rc} values were 0.1, 0.2, and 0.3. Bearing failure of the roughened surface was observed as a result of the test. The shear strength decreased with increasing r_N and decreasing r_{rc}. Subsequently, an expression for the shear strength of a roughened surface was proposed. In this expression, the shape of an uneven surface was regarded as a cone. To estimate the shear strengths of the hybrid joints, the shear force from the previous dowel model was added to the proposed expression. Finally, the values obtained using the calculation method were compared with the test results. It was demonstrated that the proposed expression could reasonably estimate the test results, with a correlation coefficient of 0.93. In addition, for structural designs, the proposed expression should be multiplied times 0.7 to estimate the lower limit of the test results.

Keywords: Roughened concrete surface; Bearing failure; Dowel action; Seismic retrofit; Combined stress

1 INTRODUCTION

Recently, decarbonization has become one of the most important global environmental issues; hence, instead of building new structures, it is important to use existing structures. In this regard, seismic retrofitting is required for seismically poor reinforced concrete (RC) structures. In such structures, new members are connected to existing members using post-installed dowel bars and roughened concrete surfaces. In this report, a joint consisting of a roughened surface and post-installed dowel bar is called a hybrid joint.

During an earthquake, because shear stress is transferred through the joints, the structural design of the joints is essential. **Fig. 1** depicts examples of roughened concrete surfaces. The shape of the shear key [1] is regular; therefore, it is easy to estimate the shear strength. However, shear keys are generally manufactured before concrete placement; thus, it is difficult to apply shear keys to existing structures. Hence, for existing RC structures, a water jet [2] or vibration hammer [3-5] is used to roughen the concrete surface. As shown in **Fig. 1** (b), the surface can be entirely roughened by a water jet; therefore, interlocking is effective. Nevertheless, on a surface with a vibration hammer, the effect of interlocking is small because the surface is partially roughened, as shown in **Fig. 1** (c). However, for some RC buildings, abundant water cannot be used during retrofitting construction because household items in other rooms may be broken by water. Therefore, it is important to evaluate the surface using a vibration hammer for

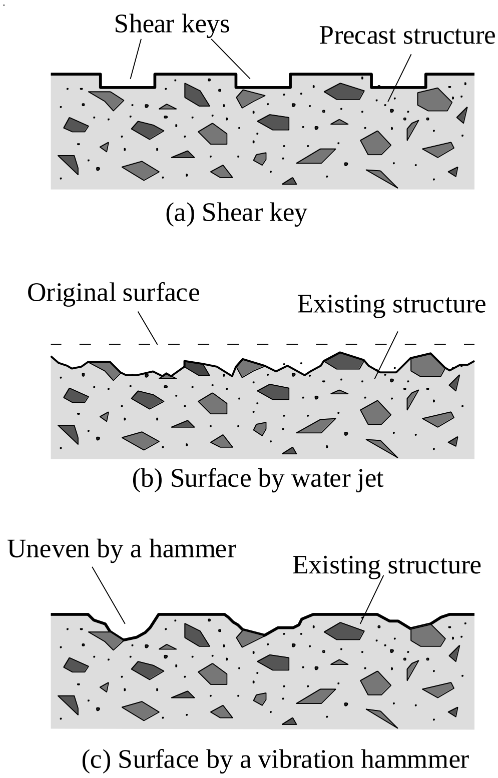

Fig. 1 Examples of joint surfaces

seismic retrofitting.

Fig. 2 shows an example of a building that is seismically retrofitted using an outside frame [6]. In such buildings, new members are attached to the existing frame through an expanded slab, as shown in the cross-section presented in **Fig. 2**. This technique is useful in buildings with balconies or outside corridors. However, during an earthquake, the joints are subjected to shear and tensile stresses owing to the bending moment of the expanded slab. Therefore, a technique to estimate the shear strength of a joint under combined stress is required.

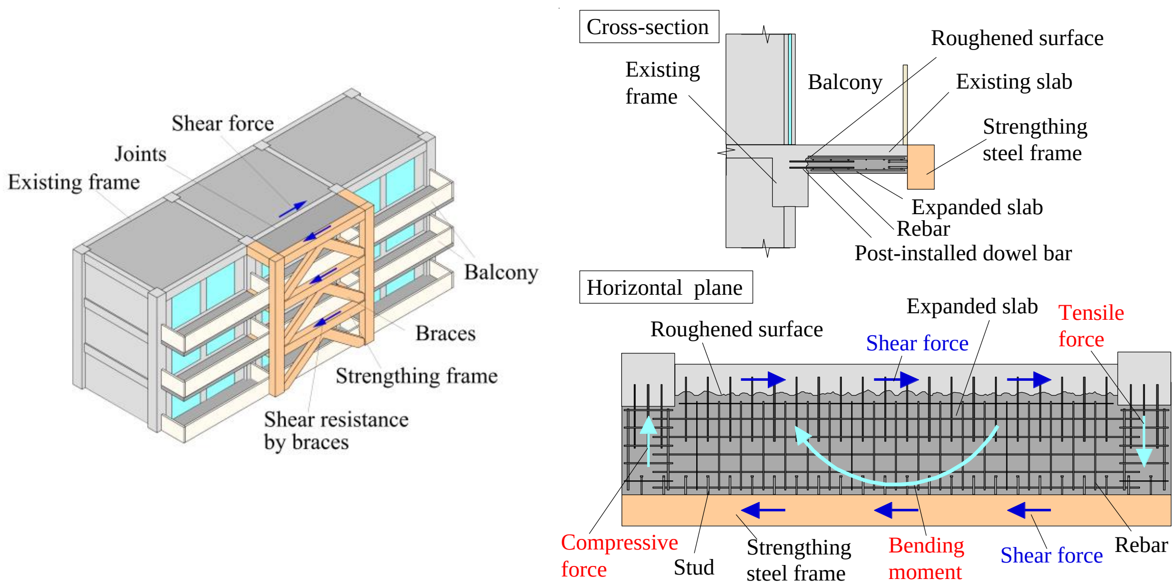

Fig. 2 Example of a structure seismically retrofitted using an outside frame.

Although seismic retrofitting is a recent research topic, the shear resistance of roughened concrete surfaces is a classical research topic. In the 1960s, the shear-friction theory was developed in representative studies focusing on roughened surfaces and dowel bars [7,8]. Santos and Júlio [9] reviewed the design expressions for shear-friction theory, discussing studies from 1960 [10] to 2011 [11]. Although the shear resistance of a roughened surface was initially regarded as friction, aggregate interlocking [12-18] has been considered since the 1980s. For example, Walraven modeled a cracked surface by considering an aggregate as a spherical body [14,15]. In addition, Bujadaham proposed a contact density function [16,17], which expresses the density of the uneven angle of the local surface. Dowel bars have been used in precast structures [19-23], whereas post-installed anchors [24,25] and reinforcing bars [26,27] have been used in retrofitted structures. Furthermore, joints with roughened surfaces and dowel bars have been investigated [28-30]. Xia et al. [30] investigated the interactions between the shear keys and reinforcing bars via direct shear tests; subsequently, the percentages of cohesion, friction, and dowel action on the shear stress–displacement relationship were explained. Further, Ghayeb reviewed dowel joints for precast structures [23].

Additionally, the authors studied roughened surfaces and dowel actions. The shear strengths [3] and mechanical behaviors [4,5] of roughened concrete surfaces and dowel models of post-installed anchors [31-33] have been investigated. For post-installed dowel bars, the behavior under combined stress was investigated, whereas that of roughened surfaces was not investigated. Moreover, the design expressions of post-installed anchors and reinforcing bars have been used in some design codes [25,27,34,35], whereas those of roughened surfaces manufactured using hammers have not been presented. As mentioned earlier, roughened concrete surfaces and dowel bars have been extensively investigated; however, studies focusing on roughened surfaces using vibration hammers and behaviors under combined stresses are limited. In the present research, shear loading tests were performed on hybrid joints in which shear and normal stresses were applied. Moreover, a strength formula that can estimate the maximum shear force considering the tensile stress was proposed. Section 2 describes the test plan, Section 3 presents the test results. Then, in Section 4, the proposed expression is described; finally, Section 5 discusses an accuracy of the proposed expression.

Nomenclature

A_j: area of joint surface
A_{hrc}: horizontal projection area of roughened surface
$A_{hrc,1}$: horizontal projection area of one uneven surface
A_{vrc}: vertical projection area of roughened surface
$A_{vrc,1}$: vertical projection area of one uneven surface
COV: coefficient of variation
d_d: diameter of dowel bar
d_h: diameter of drilling hole
D_{max}: maximum depth of roughened surface
E_C: Young's modulus of concrete
E_G: Young's modulus of grout
E_S: Young's modulus of dowel bar
f_C: compressive strength of concrete
f_C': specified compressive strength of concrete
f_G: compressive strength of grout
f_y: yield strength of dowel bar
L_e: embedded length of dowel bar
p: allowable tensile force of dowel bar
p_u: ultimate tensile strength of dowel bar
q: allowable shear force of dowel bar
q_u: ultimate shear strength of dowel bar
r: radius of cone
Q: shear force in the test
Q_d: shear strength of dowel bar calculated by the previous model [33]
Q_{hj}: shear strength of hybrid joint
Q_{max}: maximum shear force in the test
Q_{rc}: shear strength of roughened surface proposed in this study
Q_s: shear strength of roughened surface in the previous study [3]
r_N: tensile ratio
r_{rc}: roughened concrete area ratio (ratio of A_{hrc} to A_j)
δ: shear displacement
δ_{max}: shear displacement at Q_{max}
$\delta_{max,\ ave}$: average value of δ_{max}
ρ: coefficient of correlation
σ_0: compressive normal stress
τ_{rc}: shear stress of roughened surface according to the proposed expression
$\tau_{max,rc}$: maximum shear stress of roughened surface in the test

2 DETAILS OF THE SHEAR LOADING TEST

The primary objective of this study was to investigate the shear strengths of hybrid joints subjected to normal and shear forces. The details of the tests performed are provided below.

2.1 *Test parameters*

Table 1 lists the material properties of the dowel bars, concrete, and grout. Material testing was performed according to the Japanese Industrial Standard [36,37].

The test parameters of the specimens were: the roughened concrete area ratio r_{rc}, diameter of the dowel bar d_d, and normal stress, where r_{rc} is the ratio of the horizontal projection area of the uneven area A_{hrc} to the joint area A_j. Based on the previous studies [3-5], the bearing and shear failures were identified as the failure modes. Considering the bearing failure, the uneven side was observed to be damaged, as shown in **Fig.3** (a). Therefore, the maximum shear stress depends on the concrete bearing stress. Considering the shear failure, the concrete and grout were observed to be horizontally fractured, as shown in **Fig.3** (b). Thus, the maximum shear stress depends on the shear strength of the concrete and grout. The bearing failure mode was observed when r_{rc} = 0.1–0.3, and the shear failure mode was observed when r_{rc} > 0.5 [4]. In addition, the shear strength increased as r_{rc} increased; however, it became almost constant with r_{rc} = 0.3 and greater. Hence, in this study, the bearing failure mode was focused on, and r_{rc} was set to 0.1, 0.2, and 0.3. In this test, a normal stress was applied to the specimens. The compressive normal stress σ_0 was set to –0.48 N/mm^2 [3-5]. Meanwhile, the tensile stress ratio r_N was set to 0, 0.33, and 0.66, as in the previous tests [32,33]. Here, r_N is the ratio of the tensile stress to the yield strength of the dowel bar f_y (N/mm^2). d_d (mm) was set to 13, 16, and 19 mm, and the compressive strength of concrete f_c (N/mm^2) was set to 20 N/mm^2. These values are applied to most joints in seismically retrofitted structures.

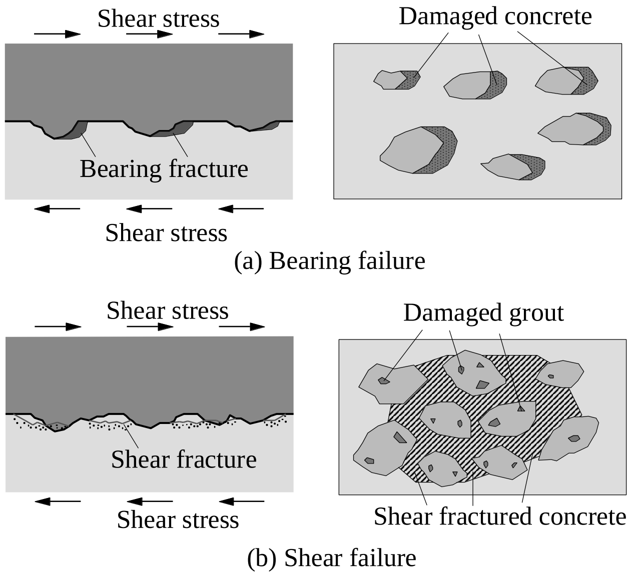

Fig. 3 Mechanisms of bearing and shear failure.

2.2 *Characteristics of specimens for the shear loading test*

Figs. 4 and **5** show the details of the specimen and photographs captured during their construction, respectively. The specimen size was the same as that used in the previous tests [33]. The concrete block dimensions of the specimens were 440 mm × 460 mm × 250 mm. As the concrete was vertically cast, the surfaces of the joint sides had a smooth finish with plywood as the formwork. The ratios of the longitudinal and transverse bars in the concrete block were 0.74% and 0.28%, respectively, and those of the grout block were 0.75% and 0.76%, respectively. These values were determined to model a normal RC beam or column and the joint of a seismically retrofitted building. After air-drying for 28 d, the specimen surfaces were roughened using a vibration hammer, and r_{rc} was determined via image analysis [3,4], as shown in **Figs. 5** (a) and (b). The results of the image analysis are presented in **Table 1**. The measured r_{rc} values are similar to the target r_{rc} values.

Table 1
Parameters of the shear loading test. In the specimen IDs, D, R, C, and T indicate the dowel bar, roughened ratio, and compressive and tensile stresses, respectively, and the numerical values represent d_d, r_{rc}, σ_0, or r_N, and the serial number. d_h is the diameter of drilling hall (mm). E_s, E_c, and E_G are the Young's modulus (kN/mm²) of the dowel bar, concrete, and grout, and f_c and f_G are the compressive strength (N/mm²) of the concrete and grout, respectively. Here, D_{max} is the maximum depth of the roughened surface (mm).

Specimen ID	σ_0 / r_N	r_{rc}		Dowel bar					Concrete		Grout		D_{max}
		Target	Measured	d_d	Num.	d_h	f_y	E_s	f_C	E_C	f_G	E_G	
D13R01C$_{048}$-1	–0.48	0.1	0.107	13	1	16	403	174	22.5	17.4	68.0	25.9	–
D13R01C$_{048}$-2	–0.48	0.1	0.115	13	1	16	403	174	22.5	17.4	68.0	25.9	–
D13R02C$_{048}$	–0.48	0.2	0.206	13	1	16	403	174	20.1	21.8	69.2	27.2	–
D13R03C$_{048}$	–0.48	0.3	0.316	13	1	16	403	174	22.5	17.4	68.0	25.9	–
D16R01C$_{048}$-1	–0.48	0.1	0.093	16	1	22	376	170	22.5	17.4	68.0	25.9	–
D16R01C$_{048}$-2	–0.48	0.1	0.107	16	1	22	387	187	20.1	21.8	69.2	27.2	–
D16R02C$_{048}$	–0.48	0.2	0.190	16	1	22	387	187	20.1	21.8	69.2	27.2	–
D16R03C$_{048}$	–0.48	0.3	0.302	16	1	22	387	187	20.1	21.8	69.2	27.2	–
D13R01T$_{000}$	0.00	0.1	0.098	13	1	16	381	171	23.0	17.5	65.6	26.4	12.0
D13R01T$_{033}$	0.33	0.1	0.106	13	1	16	381	171	23.0	17.5	65.6	26.4	11.5
D13R01T$_{066}$	0.66	0.1	0.107	13	1	16	381	171	23.0	17.5	65.6	26.4	11.0
D13R02T$_{000}$	0.00	0.2	0.194	13	1	16	381	171	23.0	17.5	65.6	26.4	12.0
D13R02T$_{033}$	0.33	0.2	0.210	13	1	16	381	171	23.0	17.5	65.6	26.4	12.0
D13R02T$_{066}$	0.66	0.2	0.199	13	1	16	381	171	23.0	17.5	65.6	26.4	12.5
D13R03T$_{000}$	0.00	0.3	0.300	13	1	16	381	171	23.0	17.5	65.6	26.4	11.0
D13R03T$_{033}$	0.33	0.3	0.318	13	1	16	381	171	23.0	17.5	65.6	26.4	18.0
D13R03T$_{066}$	0.66	0.3	0.304	13	1	16	381	171	23.0	17.5	65.6	26.4	12.0
D16R01T$_{000}$	0.00	0.1	0.093	16	1	22	387	175	20.8	16.4	62.9	24.4	11.5
D16R01T$_{033}$	0.33	0.1	0.094	16	1	22	387	175	20.8	16.4	62.9	24.4	11.3
D16R01T$_{066}$	0.66	0.1	0.106	16	1	22	387	175	20.8	16.4	62.9	24.4	13.0
D16R02T$_{000}$	0.00	0.2	0.196	16	1	22	387	175	20.8	16.4	62.9	24.4	13.0
D16R02T$_{033}$	0.33	0.2	0.199	16	1	22	387	175	20.8	16.4	62.9	24.4	11.5
D16R02T$_{066}$	0.66	0.2	0.210	16	1	22	387	175	20.8	16.4	62.9	24.4	13.0
D16R03T$_{000}$	0.00	0.3	0.301	16	1	22	387	175	20.8	16.4	62.9	24.4	12.9
D16R03T$_{033}$	0.33	0.3	0.294	16	1	22	387	175	20.8	16.4	62.9	24.4	15.0
D16R03T$_{066}$	0.66	0.3	0.292	16	1	22	387	175	20.8	16.4	62.9	24.4	15.0
D19R01T$_{000}$	0.00	0.1	0.095	19	1	25	391	176	23.0	17.5	65.6	26.4	12.0
D19R01T$_{033}$	0.33	0.1	0.102	19	1	25	391	176	23.0	17.5	65.6	26.4	13.0
D19R01T$_{066}$	0.66	0.1	0.096	19	1	25	391	176	23.0	17.5	65.6	26.4	11.0
D19R02T$_{000}$	0.00	0.2	0.215	19	1	25	391	176	23.0	17.5	65.6	26.4	13.0
D19R02T$_{033}$	0.33	0.2	0.203	19	1	25	391	176	23.0	17.5	65.6	26.4	13.5
D19R02T$_{066}$	0.66	0.2	0.204	19	1	25	391	176	23.0	17.5	65.6	26.4	10.5
D19R03T$_{000}$	0.00	0.3	0.307	19	1	25	391	176	23.0	17.5	65.6	26.4	14.5
D19R03T$_{033}$	0.33	0.3	0.304	19	1	25	391	176	23.0	17.5	65.6	26.4	13.0
D19R03T$_{066}$	0.66	0.3	0.304	19	1	25	391	176	23.0	17.5	65.6	26.4	12.5
												Ave.	12.6

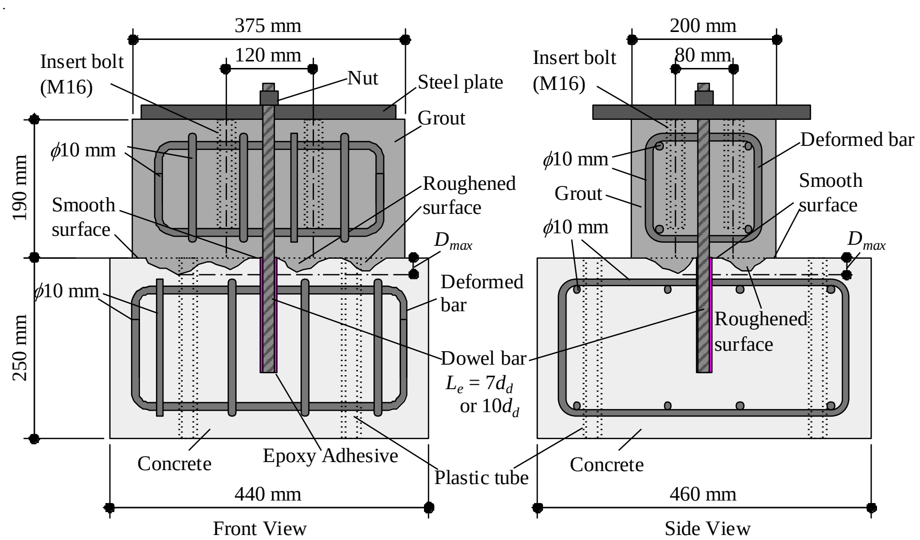

Fig. 4 Characteristics of the specimens for shear loading tests. The embedded length of the dowel bar L_e is $7d_d$ and $10d_d$ for the specimens subjected to compressive and tensile normal stresses, respectively.

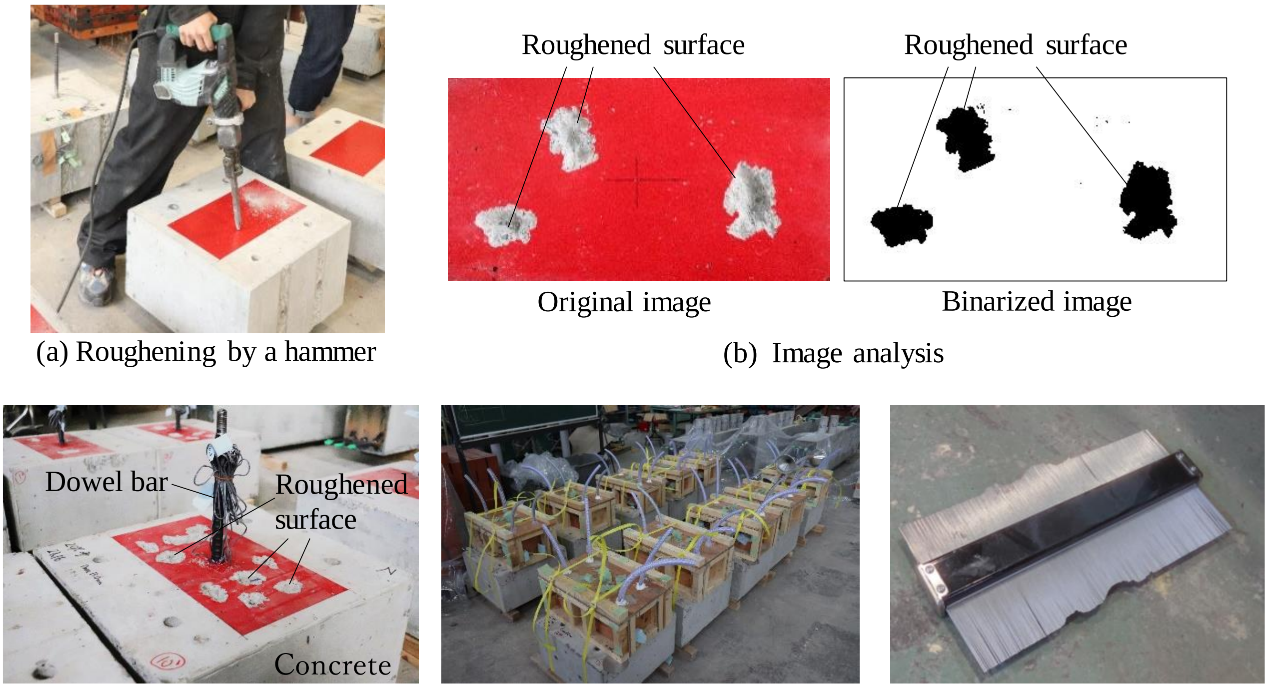

(a) Roughening by a hammer (b) Image analysis

(c) Joint surface (d) Formwork of the new side (e) Shape-measuring gauge

Fig. 5 Specimen construction.

For the specimens subjected to the tensile normal stress, the maximum depths of the roughened surface D_{max} were measured using a shape-measuring gauge, as shown in **Fig. 5** (e). Similar to the previous study, the target depth was set to 10 mm in this study [3]. Furthermore, the measured depth was 11.0–18.0 mm and the average depth was 12.6 mm, as shown in **Table 1**.

After roughening, a hole was bored at the position of the post-installed dowel bar using a diamond core drill. Subsequently, the dowel bar was adhered using an epoxy adhesive [31-33]. **Fig. 5** (c) depicts the joint surface. After the adhesive hardened, grease was applied to the smooth surface to minimize friction. Then, the reinforcing bars were appropriately arranged, and the formwork of the new side was set, as shown in **Fig. 5** (d). After that, a premixed cementitious grout was cast. The dimensions of the grout block were 375 mm × 200 mm × 190 mm.

2.3 *Loading and measuring setup*

Figs. 6 to **8** illustrate the loading setup, the loading cycles, and the setup for measuring the displacement, respectively, which are the same as those used in the previous tests [33]. In the loading setup shown in **Fig. 6**, two 150 kN screw jacks and a 500 kN hydraulic jack were employed. Using the two screw jacks, the loading beam was moved parallel to the surface during shear loading. The PID (Proportional, Integral, Differential) auto-control was applied to the vertical system. When the loading beam was forced to be parallel with the two vertical displacements measured, the values of the two normal loads for the load cells attached to the two jacks were different. Therefore, the two jacks were vertically moved using the PID auto-control such that the sum of the two loads was equal to the target normal stress.

A static shear load was applied to the specimen at a loading rate of 0.02–0.04 mm/s. In this test, the cyclic shear load was applied to the specimens, as shown in **Fig. 7**. The loading cycle was ±0.125, ±0.25, ±0.50, ±1.0, ±1.5, ±2.0, ±3.0, ±4.0, ±6.0, and ±8.0 mm. For δ = 0.5–4.0 mm, the number of repetition was two for the same displacement. During shear loading, the surface was moved horizontally and vertically; therefore, the slip and opening of the surface were measured using the four displacement sensors depicted in **Fig. 8**.

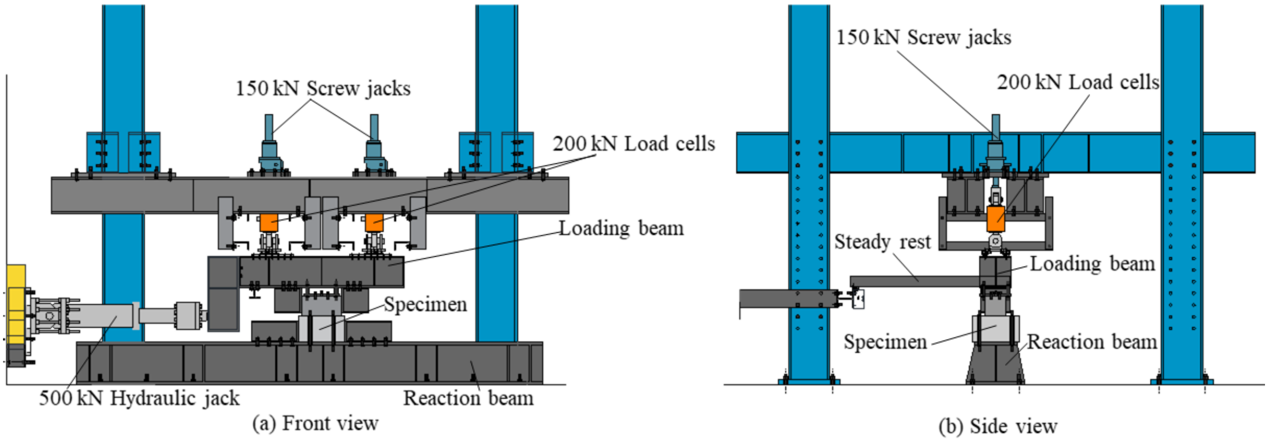

(c) Photograph

Fig. 6 Loading setup [33].

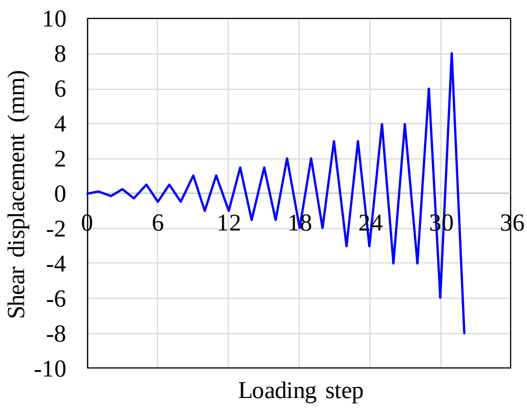

Fig. 7 Loading regime.

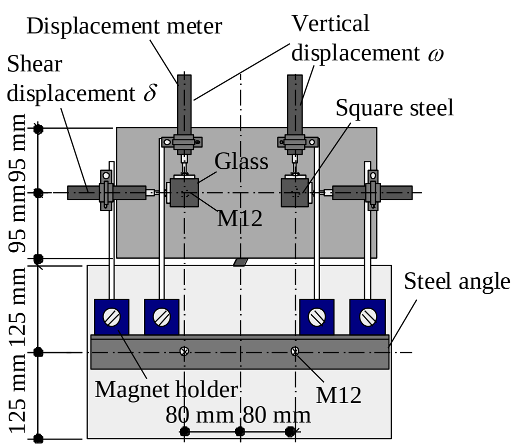

Fig. 8 Setup for measuring displacement [33].

3 TEST RESULTS

3.1 *Failure mode*

Fig. 9 provides examples of the failure modes.

As mentioned earlier, there are two failure modes for the roughened surfaces: bearing and shear failures [4]. Because r_{rc} was set to 0.1–0.3 in this test, it was predicted that bearing failure would occur. As shown in **Fig. 9**, the sides of each uneven surface broke after loading. Moreover, the damaged grout barely remained on the uneven concrete surface. For shear failure, the grout and concrete failed; therefore, the damaged grout remained in the concrete, as shown in **Fig. 3** (b). Hence, it was considered that the failure mode of this test was bearing failure, as shown in **Fig. 3** (a).

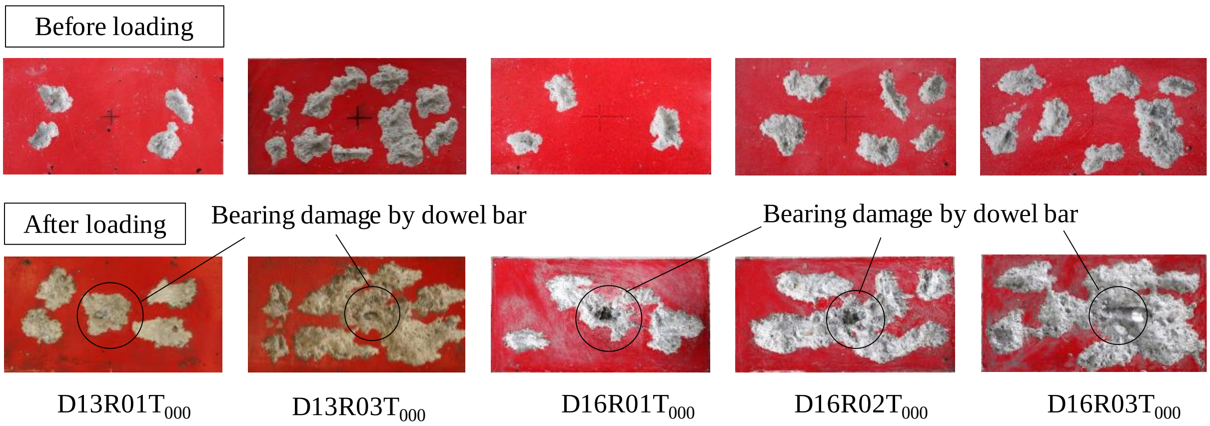

Fig. 9 Specimen failure modes.

3.2 *Shear strength*

Fig. 10 compares Q_{max} in different scenarios by focusing on the normal stress, and **Table 2** lists the test results for all the specimens. As shown in **Fig. 10**, Q_{max} increases with increasing r_{rc}. In addition, as the normal stress increases from compressive stress to tensile stress, Q_{max} decreases for most specimens. For the specimens with $\sigma_0 = -0.48$ N/mm^2, the range of Q_{max} is 102.5–161.5 kN, whereas for the specimens with $r_N = 0.66$, it is 28.7–73.9 kN. Thus, with tensile normal stress of $r_N = 0.66$, the values of Q_{max} become approximately 1/2 to 1/4 times those of the specimens subjected to compressive normal stress. In contrast, for some specimens, as the normal stress increases, Q_{max} increases, as in the results indicated by the black circles in **Fig. 10**. These irregular specimens are referred to as D13R01T033, D16R01T033, and D16R03T000. The D_{max} values for these specimens are 11.5, 11.3, and 12.9 mm. These depths are not irregular because the average depth is 12.6 mm, the coefficient of variation is 13 %, and the range is 11.0–18.0 mm. In addition, the impact of depth of the roughened surface on the shear stress was reported to be insignificant [4]. Therefore, it is considered that Q_{max} varied because of the irregular shapes properties of the roughened surfaces, except for D_{max}.

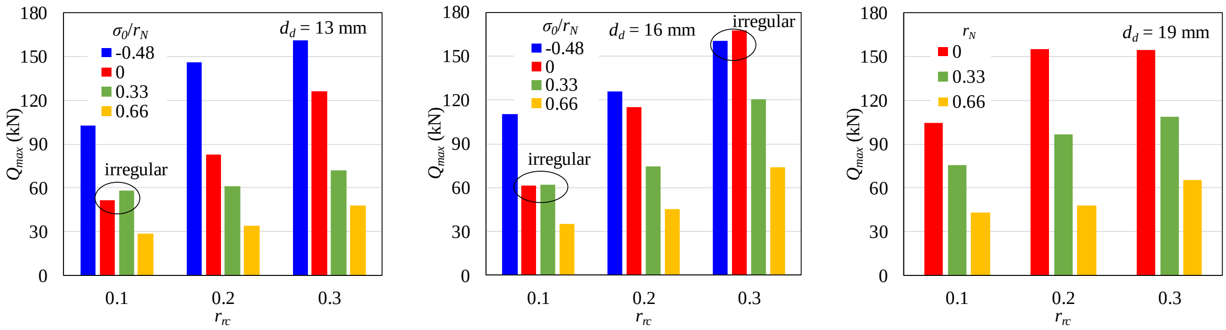

(a) d_d = 13 mm (b) d_d = 16 mm (c) d_d = 19 mm

Fig. 10 Comparison of Q_{max}.

Table 2
Shear displacements and maximum shear forces in the tests.

Specimen ID	$+\delta$ (mm)	$+Q_{max}$ (kN)	$-\delta$ (mm)	$-Q_{max}$ (kN)
D13R01C$_{048}$-1	0.25	102.5	–0.25	–89.6
D13R01C$_{048}$-2	0.25	112.1	–0.50	–93.3
D13R02C$_{048}$	0.25	146.0	–0.25	–137.8
D13R03C$_{048}$	0.27	161.5	–0.20	–145.3
D16R01C$_{048}$-1	0.50	110.5	–0.52	–111.9
D16R01C$_{048}$-2	0.42	113.5	–0.25	–100.3
D16R02C$_{048}$	0.23	126.0	–0.16	–133.3
D16R03C$_{048}$	0.90	160.3	–0.40	–143.9
D13R01T$_{000}$	0.48	51.7	–0.45	–53.7
D13R01T$_{033}$	0.47	57.8	–0.42	–42.6
D13R01T$_{066}$	0.48	28.7	–0.50	–26.6
D13R02T$_{000}$	0.20	82.8	–0.27	–76.9
D13R02T$_{033}$	0.43	61.1	–0.26	–55.5
D13R02T$_{066}$	0.46	33.9	–0.25	–32.7
D13R03T$_{000}$	0.24	126.1	–0.24	–118.6
D13R03T$_{033}$	0.50	72	–0.39	–69.7
D13R03T$_{066}$	0.25	47.8	–0.25	–49.7
D16R01T$_{000}$	0.95	61.4	–0.50	–56.9
D16R01T$_{033}$	0.49	62.0	–0.50	–67.1
D16R01T$_{066}$	0.48	35.1	–0.25	–37.0
D16R02T$_{000}$	0.48	115.1	–0.25	–93.8
D16R02T$_{033}$	0.50	74.7	–0.24	–86.3
D16R02T$_{066}$	0.50	45.3	–0.25	–44.4
D16R03T$_{000}$	0.48	167.8	–0.25	–142.9
D16R03T$_{033}$	0.41	120.2	–0.25	–97.0
D16R03T$_{066}$	0.21	73.9	–0.70	–33.4
D19R01T$_{000}$	0.95	104.5	–0.49	–99.3
D19R01T$_{033}$	0.39	75.7	–1.00	–57.1
D19R01T$_{066}$	0.88	42.8	–0.5	–42.5
D19R02T$_{000}$	0.25	155.2	–0.25	–130.0
D19R02T$_{033}$	0.93	96.4	–0.49	–89.8
D19R02T$_{066}$	0.47	47.8	–0.49	–41.7
D19R03T$_{000}$	0.25	154.6	–025	–142.3
D19R03T$_{033}$	0.50	108.5	–0.5	–107.2
D19R03T$_{066}$	0.47	65.4	–0.25	–62.8
Average	0.46	—	–0.37	—

3.3 *Load–displacement relations*

Fig. 11 shows the Q–δ envelope curves on the positive side. As listed in **Table 2**, the range of $+\delta_{max}$ is 0.21–0.50 mm for most specimens. Meanwhile, for D16R03C$_{048}$, D16R01T$_{000}$, D19R01T$_{000}$, D19R01T$_{066}$, and D19R02T$_{033}$, the range of $+\delta_{max}$ is 0.88–0.95 mm. The average value of $+\delta_{max}$ is 0.46 mm.

Observing **Fig.11,** after Q_{max}, Q decreases; subsequently, Q converges at a roughly fixed shear load. Generally, the shear load of the dowel bars increases with increasing δ [32,33], and the shear displacement during the peak load of a dowel bar is much higher than that in this test. Thus, the shear displacement should be considered for the estimation of Q_{max} of hybrid joints.

Considering the specimens' behaviors after crossing the peak shown **Fig. 11** (a), (d) and (g), the Q decreases at a relatively low rate than the other specimens. Hence, it can be inferred that because r_{rc} was small, the mechanical behavior exhibited by the dowel bar indicated better performance. In addition, the greater the r_N, the stress reduction is more insignificant in the shear load after Q_{max}.

Moreover, considering the post-peak behavior of the specimen, Q of $\sigma_0 = -0.48$ N/mm², is considerably higher than that of other specimens, as shown in **Fig. 11** (a)-(f). Thus, it is considered that the frictional resistance was caused by the compressive normal stress.

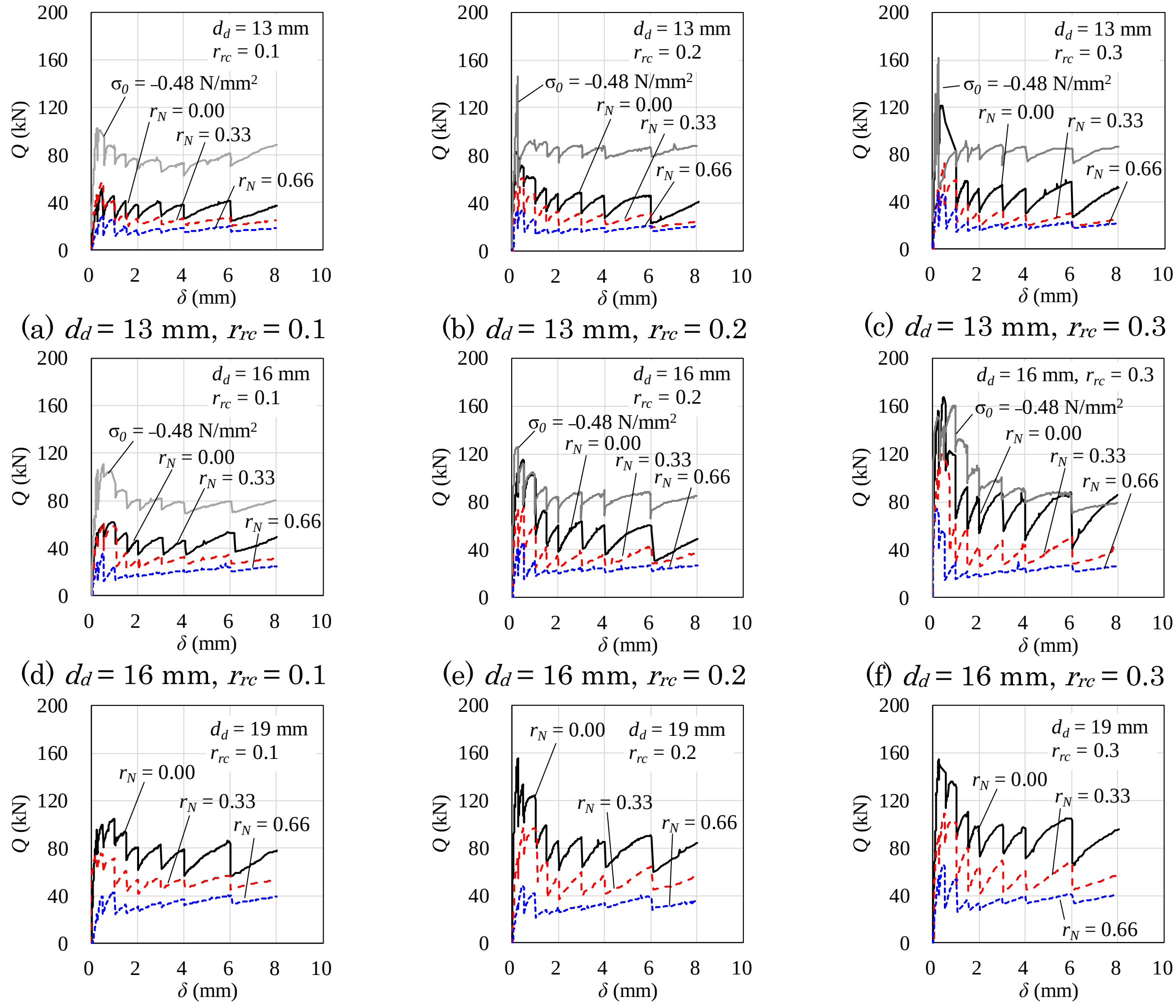

(a) $d_d = 13$ mm, $r_{rc} = 0.1$ (b) $d_d = 13$ mm, $r_{rc} = 0.2$ (c) $d_d = 13$ mm, $r_{rc} = 0.3$

(d) $d_d = 16$ mm, $r_{rc} = 0.1$ (e) $d_d = 16$ mm, $r_{rc} = 0.2$ (f) $d_d = 16$ mm, $r_{rc} = 0.3$

(g) $d_d = 19$ mm, $r_{rc} = 0.1$ (h) $d_d = 19$ mm, $r_{rc} = 0.2$ (i) $d_d = 19$ mm, $r_{rc} = 0.3$

Fig. 11 Q–δ envelope curves.

4 SHEAR STRENGTH ESTIMATION

4.1 *Previous dowel model*

In this study, the dowel model previously proposed by the authors [33] was used to estimate Q_{max}. This section briefly outlines the model. **Fig. 12** shows an image of the dowel model. The shear force Q_d is expressed as follows:

$$Q_d = q_s + q_B + q_T^S, \tag{1}$$

where q_S is the shear force owing to the bending moment of the plastic hinge; q_B is the integral value of the bearing stress; q_T^S is the shear force exerted by catenary action; and q_S, q_B, and q_T^S are calculated using M_s, σ_b, and σ_t, respectively, as illustrated in **Fig. 12**. Using this model, the shear force of the dowel bar is estimated based on the shear displacement.

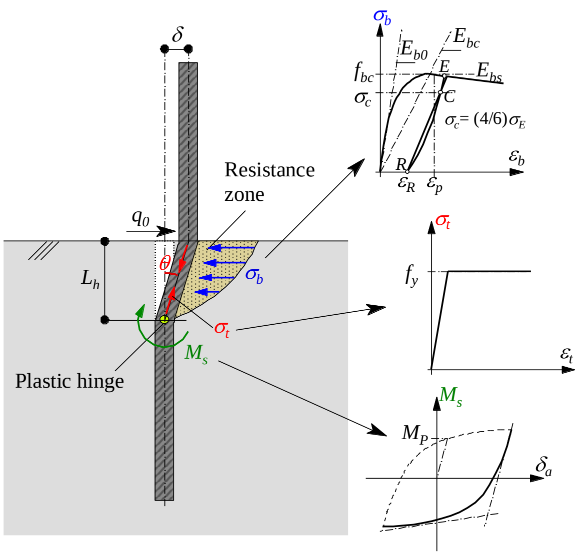

Fig. 12 Image of the dowel model. σ_b is the bearing stress of concrete, M_s is the full plastic bending moment at the plastic hinge, and σ_t is the tensile stress of the anchor bolt owing to the catenary action [33].

4.2 *Motivation for constructing a new shear strength formula for a roughened surface*

In a previous study, a shear strength formula was proposed [3]. The shear strength Q_s can be estimated by using the following equation.

$$Q_s = 4.2 \times (f_C \times E_C)^{0.17} \times A_{vrc}, \tag{2}$$

where the values of 4.2 and 0.17 are the experimental coefficients obtained using the least-squares method, A_{vrc} is the vertical projection area of the roughened surface. As shown in Eq. (2), Q_s is proportional to A_{vrc} and the exponential function $f_C \times E_C$. However, in this equation, A_{vrc} is applied, which is measured using shape measurement data with a laser displacement sensor; therefore, it is difficult to use this equation in structural designs. In addition, this formula can only be used under normal compressive stress. Hence, in this study, a new shear strength formula for a roughened surface was proposed based on Eq. (2).

4.3 *Shear strength formula for r_N* = 0.00

Because the uneven shape was manufactured using a vibration hammer, the shape was similar to a cone; therefore, in this study, the uneven shape was modeled as a cone, as shown in **Fig. 13**. Using this model, the vertical projection area of one uneven surface $A_{vrc,1}$ can be expressed as follows:

$$A_{vrc,1} = r \times D_{max}. \tag{3}$$

Here, because the horizontal projection area of one uneven surface is $A_{hrc,1} = \pi r^2$, the radius r of an uneven surface can be calculated as follows:

$$r = \sqrt{\frac{A_{hrc,1}}{\pi}}. \tag{4}$$

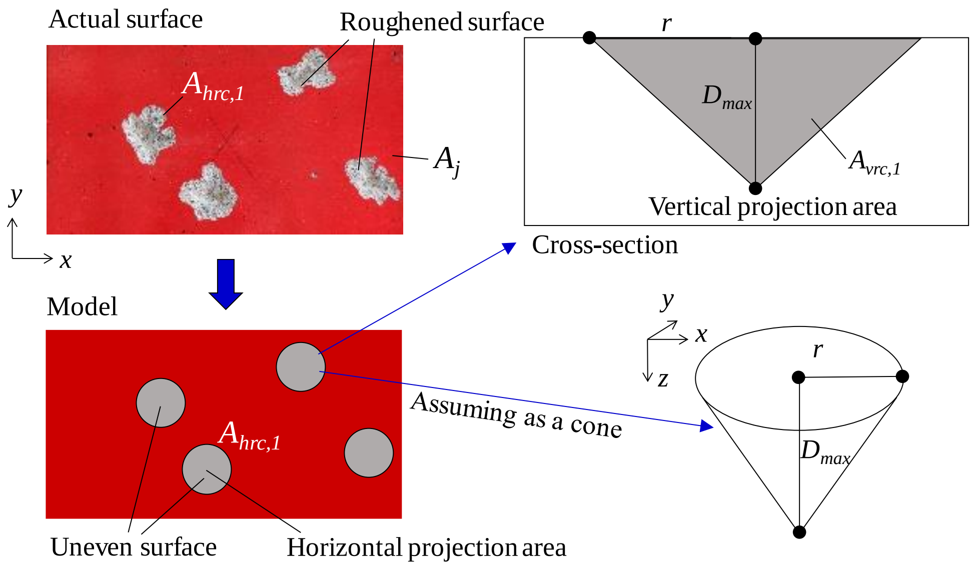

Fig. 13 Conceptual schematic of the proposed shear strength formula.

From Eq.(2), Q_{rc} can be expressed using the expression: $A_{vrc}\times(E_c\times f_c)^{0.17}$. Moreover, E_C is often expressed using a function of f_C. For instance, according to ACI 318 [34] and Eurocode 2 [38], E_C is calculated using the following equations:

$$E_C = 57{,}000\sqrt{f_C{}'}\ \text{(in psi)} \tag{5}$$

$$E_C = 33(f_C{}'/10)^{0.3}\ \text{(in MPa)}, \tag{6}$$

where $f_C{}'$ is the specified compressive strength of concrete. Here, the values of the exponent are 0.5 and 0.3. In this paper, by using the medium value of the aforementioned values, E_C is expressed as the function of $f_C{}^{0.4}$, and Q_{rc} can be expressed as follows:

$$Q_{rc} = f(A_{vrc}\cdot f_C^{0.24}). \tag{7}$$

The number of uneven surfaces N_u can be calculated by dividing $A_j\times r_{rc}$ by $A_{hrc,1}$:

$$N_u = \frac{A_j\cdot r_{rc}}{A_{hrc,1}}. \tag{8}$$

Using Eqs. (3)–(8), τ_{rc} and A_{vrc} can be expressed as follows:

$$\tau_{rc} = \frac{dQ_{rc}}{dA} = f'(A_{vrc}\cdot f_C^{0.24}) \tag{9}$$

$$A_{vrc} = A_{vrc,1}\times N_u = \frac{D_{max}r_{rc}}{\sqrt{A_{hrc,1}\pi}}. \tag{10}$$

Based on the surfaces of the specimens, $A_{hrc,1}$ is approximately 2000 mm^2. As mentioned in Section 2.2, the average value of D_{max} is 12.6 mm; thus, D_{max}= 12.6 is applied to Eq. (10) in this study. **Fig. 14** shows the relation between $\tau_{max,rc}$ and $\frac{D_{max}r_{rc}}{\sqrt{2000\pi}}f_C^{0.24}$of the specimen with r_N= 0.00. $\tau_{max,rc}$ is given by the following equation.

$$\tau_{max,rc} = (Q_{max} - Q_d)/A_j, \tag{11}$$

where Q_d is the value calculated based on $\delta_{max,\,ave}$ using the dowel model [33] and $\delta_{max,\,ave}$ = 0.46 mm from **Table 2**.

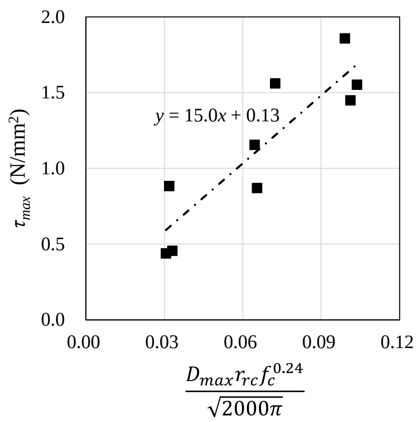

Fig. 14 $\tau_{max,rc}$–$A_{vcr}\cdot f_c^{0.24}$ relation; R refers to the correlation coefficient.

The regression line is obtained from **Fig.14**. Moreover, because the calculated value of $15.0/\sqrt{2000}$ is approximately 1/3, τ_{rc} can finally be expressed as follows:

$$\tau_{rc} = \frac{r_{rc}D_{max}}{3\sqrt{\pi}}f_C^{0.24} + 0.13. \tag{12}$$

4.4 *Application to various normal stresses*

The strength under tensile stress was also considered. Although the relationship between the shear and tensile strengths of a roughened concrete surface has not been previously presented, that of anchors has been described in previous articles [32,33] and design codes [34,35]. The following equations are often used in design codes and previous articles:

$$\left({}^{p}/_{p_u}\right)^{\alpha} + \left({}^{q}/_{q_u}\right)^{\alpha} = 1 \tag{13}$$

$$q = q_u \sqrt[\alpha]{1 - \left({}^{p}/_{p_u}\right)^{\alpha}}, \tag{14}$$

where p and q are the allowable tensile and shear forces under the combined stress, respectively, and p_u and q_u denote the ultimate tensile and shear forces, respectively. In this study, Eq. (14) was applied to the roughened concrete surface and extended to the compressive normal stress.

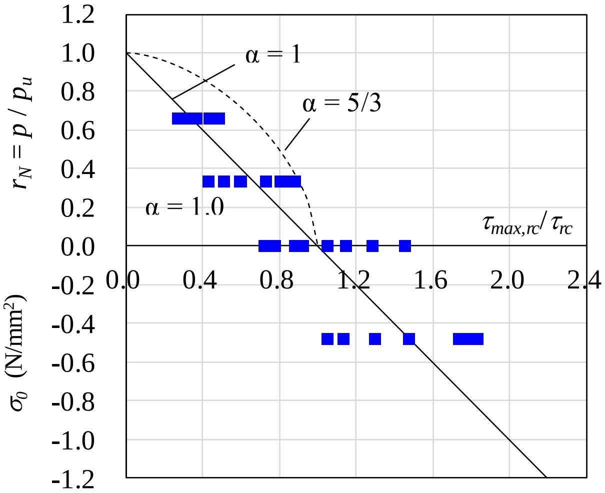

Fig. 15 Normal–shear stress interaction.

Fig. 15 shows the normal–shear stress interactions of the specimens. Typically, α is set as 5/3 [34,35]. However, as shown in **Fig. 15**, the curve with $\alpha = 5/3$ overestimates the test results under tensile stress. Although the results of $\tau_{max,rc}/\tau_{rc}$ are scattered, the line with $\alpha = 1$ estimates the middle of the test results. Hence, α was set to 1 in this study. Therefore, τ_{rc} of the specimen under combined stress can be described as follows:

$$\tau_{rc} = \left(\frac{r_{rc} D_{max}}{3\sqrt{\pi}} f_C^{0.24} + 0.13\right)(1 - n), \tag{16}$$

where n is σ_0 or r_N for normal compressive stress or tensile stress ratio, respectively.

Finally, the shear strength of the hybrid joint under normal stress can be estimated as follows:

$$Q_{hj} = Q_{rc} + Q_d, \tag{17}$$

where $Q_{rc} = \tau_{rc} \times A_j$.

5 DISCUSSION

In this section, the calculated values obtained by the proposed estimation are compared with the test results. **Fig. 16** compares Q_{hj} and the test results, and **Table 3** lists the calculated values and ratios of Q_{max} to Q_{hj}.

As shown in **Fig. 16**, most of the test results are reasonably estimated by the proposed expression because the coefficient of correlation ρ is 0.93, and the average ratio of Q_{max} to Q_{hj} is 1.01, as shown in **Table 3**. Moreover, the COV is 15%; therefore, almost 68% of the specimens can be estimated with the range 0.85–1.15 by employing a Gaussian distribution. In addition, for structural design, a lower strength limit is required. This limit was calculated by multiplying Eq. (16) times 0.7 considering the value of twice as COV.

The ratio of Q_{rc} to Q_{hj} is shown in **Fig. 17**. When the roughened surface is subjected to compressive stress, the range of Q_{rc}/Q_{hj} *is* approximately 0.65–0.9, and Q_{rc}/Q_{hj} decreases with increasing r_N. Focusing on the results for r_{rc} = 0.3, when r_N = 0.66, the range of Q_{rc}/Q_{hj} is approximately 0.6–0.8. Thus, the roughened surface could resist the shear force for over 60% of the values of Q_{hj}, even if a tensile normal stress was applied. In addition, as r_{rc} decreases, the range of the distribution also decreases; for example, when r_{rc} = 0.1 and r_N = 0.66, the range is approximately 0.4–0.7.

As mentioned earlier, although the roughened surface was subjected to the tensile stress, the surface resisted the shear force for approximately 40%–90% of the values of Q_{hj}. Furthermore, the proposed expression reasonably estimates the shear strength of a roughened surface subjected to compressive and tensile normal stresses. Therefore, it can be concluded that the proposed expression is useful for the structural design of seismically retrofitted structures.

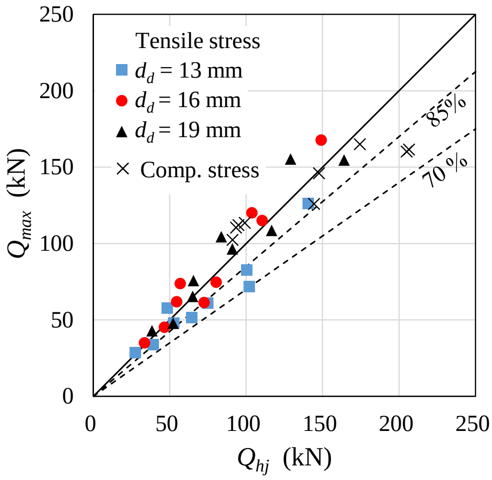

Fig. 16 Comparison of shear strength between the test results and the values from the proposed expression.

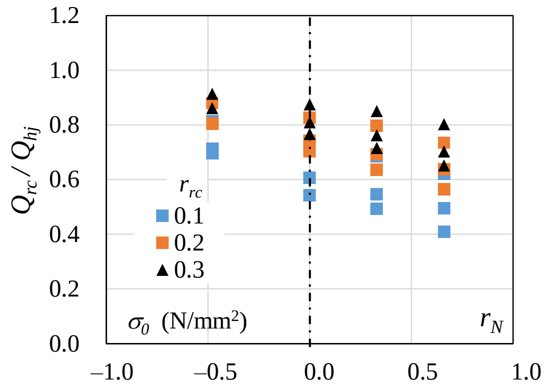

Fig. 17 Ratio of Q_{rc} to Q_{hj}.

Table 3 Results of the proposed shear strength estimation.

Specimen ID	τ_{rc} (N/mm^2)	Q_d (kN)	Q_{hj} (kN)	Q_{max} / Q_{hj}
D13R01C$_{048}$-1	0.977	14.89	91.0	1.13
D13R01C$_{048}$-2	1.029	14.89	94.9	1.18
D13R02C$_{048}$	1.732	14.89	147.7	0.99
D13R03C$_{048}$	2.517	15.24	206.5	0.78
D16R01C$_{048}$-1	0.866	29.31	93.4	1.18
D16R01C$_{048}$-2	0.941	27.83	99.0	1.15
D16R02C$_{048}$	1.547	23.04	144.4	0.87
D16R03C$_{048}$	2.354	33.79	204.9	0.78
D13R01T$_{000}$	0.623	18.01	64.3	0.80
D13R01T$_{033}$	0.443	15.62	48.4	1.20
D13R01T$_{066}$	0.227	10.68	27.4	1.05
D13R02T$_{000}$	1.106	18.01	100.5	0.82
D13R02T$_{033}$	0.794	15.62	74.8	0.82
D13R02T$_{066}$	0.384	10.68	39.2	0.87
D13R03T$_{000}$	1.639	18.01	140.5	0.90
D13R03T$_{033}$	1.158	15.62	102.1	0.71
D13R03T$_{066}$	0.564	10.68	52.7	0.91
D16R01T$_{000}$	0.587	29.21	72.5	0.85
D16R01T$_{033}$	0.396	25.34	54.4	1.14
D16R01T$_{066}$	0.221	17.32	33.5	1.05
D16R02T$_{000}$	1.092	29.21	110.4	1.04
D16R02T$_{033}$	0.742	25.34	80.3	0.93
D16R02T$_{066}$	0.395	17.32	46.5	0.97
D16R03T$_{000}$	1.608	29.21	149.1	1.13
D16R03T$_{033}$	1.054	25.34	103.8	1.16
D16R03T$_{066}$	0.532	17.32	56.7	1.30
D19R01T$_{000}$	0.606	39.35	83.7	1.25
D19R01T$_{033}$	0.430	34.14	65.4	1.16
D19R01T$_{066}$	0.209	23.33	38.4	1.12
D19R02T$_{000}$	1.209	39.35	129.0	1.20
D19R02T$_{033}$	0.770	34.14	90.9	1.06
D19R02T$_{066}$	0.393	23.33	52.2	0.92
D19SR30T$_{000}$	1.676	39.35	164.0	0.94
D19SR30T$_{033}$	1.112	34.14	116.6	0.93
D19SR30T$_{066}$	0.564	23.33	65.0	1.01
			Average	1.01
			COV (%)	15

6 CONCLUSION

In this study, shear loading tests of joints with roughened concrete surfaces and post-installed dowel bars subjected to normal and shear stresses were conducted, and an expression for shear strength was proposed. The findings of this study can be summarized as follows.

1) According to the test results, even if the roughened surface was subjected to a tensile normal stress, the surface could resist the shear force by being combined with the dowel bar. In addition, as r_N increased, the shear strength decreased. For the specimens with $r_N = 0.66$, Q_{max} was 1/2 to 1/4 times that of the specimen with $\sigma_0 = -0.48$ N/mm^2.
2) The range of the shear displacement during the maximum load was 0.21–0.95 mm, and the average displacement was 0.46 mm. These values are smaller than those of the dowel bars.
3) A new shear strength expression for a roughened concrete surface was proposed. In this expression, the unevenness of the roughened surface was regarded as a cone; additionally, f_c, D_{max}, r_{rc}, and the normal stress were considered.
4) By combining the proposed shear strength model of the roughened surface and the previous dowel model, the maximum shear force of the hybrid joints was predicted well; the correlation coefficient was 0.93, and the average ratio of Q_{max} to Q_{hj} was 1.01. In addition, for the structural designs, the lower limits were obtained by multiplying 0.7 times the proposed expression.
5) Although the joints were subjected to tensile and shear stresses, the roughened concrete surface had 40%–90% of the shear strength of the joints. Therefore, it is important to estimate the shear strength of the roughened surface.

The proposed expression can be used for $r_{rc} = 0.1$–0.3, $f_c = 20$–23 N/mm^2, $d_d = 13$–19

mm, and σ_0 = 0.00 to –0.48 N/mm^2 or r_N = 0.00–0.66. Future studies will focus on high-strength concrete and other dowel bar arrangements.

Acknowledgments

This study was supported by the Japan Society for the Promotion of Science KAKENHI (grant number JP19K04684) and partially supported by the Collaborative Research Project of the Laboratory for Materials and Structures, Institute of Innovative Research, Tokyo Institute of Technology.

References

[1] Yazdi MA, Dejager E, Debraekeleer M, Gruyaert E, Tittelboom KV, Belie ND. Bond strength between concrete and repair mortar and its relation with concrete removal techniques and substrate composition. Const Bulid Mate 2020;230:116900. (10.1016/j.conbuildmat.2019.116900)

[2] Ghayeb HH, Razak HA, Sulong NHR. Performance of dowel beam–to–column connections for precast concrete systems under seismic loads: A review. Const Build Mate 2020;237:117582. (10.1016/j.conbuildmat.2019.117582)

[3] Musya U, Katagiri Y, Takase Y, Abe T, Sakamoto K, Hiwatashi T, Katori K. Bearing strength formula of roughened concrete considering vertical projection area. J Advanc Conc Tech 2019;17:309–18. (10.3151/jact.17.309)

[4] Isozaki T, Musya U, Takase Y, Abe T, Sakamoto K, Hiwatashi T, Katori K. Mechanical model of shear stress transfer of roughened concrete surface for R/C existing member. Proc Compt Model Concr Struct 2018;973–81. (10.1201/9781315182964–112)

[5] Katagiri Y, Takase Y, Abe T, Sakamoto K, Hiwatashi T, Katori K. Mechanical model of roughened concrete of existing members for shear failure mode. Proc Fract Concr Concr Struct. 2019;235482. (10.21012/FC10.235482)

[6] Takase Y, Ikeda T, Suzumura T. Sseismic retrofitting effect of 10-story residential

building retrofitted using passive seismic control system with amplifier mechanism. 5th Inter Conf on Comp Meth in Struct Dyn and Earth Eng 2015;3934-45. (10.7712/120115.3669.1161)

[7] Hofbeck JA, Ibrahim IO, Mattock AH. Shear transfer in reinforced concrete. J ACI 1969;66(2):119–28.

[8] Mattock AH, Hawkins NM, Shear transfer in reinforced concrete recent research. PCI J 1972;17:55–75. (10.15554/pcij.03011972.55.75)

[9] Santos PMD, Júlio ENBS. A state–of–the–art review on shear–friction. Eng Struct 2012;45:435–48. (10.1016/j.engstruct.2012.06.036)

[10] Anderson AR. Composite designs in precast and cast–in–place concrete. Prog Archit 1960;41(9):172–9.

[11] Santos PMD, Júlio ENBS. Factors affecting bond between new and old concrete. ACI Mater J 2011;108(4):449–56.

[12] Bazant ZP, Gamgarova P. Rough cracks in reinforced concrete. J Struct Div 1980;106(4):819–42.

[13] Riggs HR, Powell GH. Rough crack model for analysis of concrete. J Eng Mech 1986;112(5):448–64. (10.1061/(ASCE)0733–9399(1986)112:5(448))

[14] Walraven JC. Fundamental analysis of aggregate interlock. J Struct Div 1981;107(11):2245–70. (10.1061/JSDEAG.0005820)

[15] Walraven JC, Reinhardt HW. Theory and experiments on the mechanical behaviour of cracks in plain and reinforced concrete subjected to shear loading. Heron 1981;26(1A):1–68.

[16] Bujadaham B, Maekawa K. Qualitative studies on mechanisms of stress transfer across cracks in concrete. Proc JSCE 1992;451(V–17):265–75. (10.2208/jscej.1992.451_265)

[17] Bujadaham B, Maekawa K. The universal model for stress transfer across cracks in concrete. Proc JSCE 1992;451(V–17):277–87. (10.2208/jscej.1992.451_277)

[18] Figueira D, Sousa C, Neves AS, Constitutive model for aggregate interlock in FEM analyses of concrete interfaces with embedded steel bars. Inter J Concr Struct Mater 2020;14:15. (10.1186/s40069–019–0390–8)

[19] Friberg BF. Design of dowels in the transverse joints of concrete pavements. Proc Am Soc Civ Eng 1938;64(9):1809–28.

[20] Vintzēleou EN, Tassios TP. Mathematical models for dowel action under monotonic and cyclic conditions. Mag Concr Res 1986;38(134):13–22. (10.1680/macr.1986.38.134.13)

[21] Poli SD, Prisco MD, Gambarova PG, Shear response, deformations, and subgrade stiffness of dowel bar embedded in concrete. ACI Struct J 1992;89(6):665–75.

[22] Sorensen JH, Hoang LC, Olesen JF, Fischer G. Testing and modeling dowel and catenary action in rebars crossing shear joints in RC. Eng Struct 2017;145:234–45. (10.1016/j.engstruct.2017.05.020)

[23] Ghayeb HH, Razak HA, Sulong NHR. Performance of dowel beam–to–column connections for precast concrete systems under seismic loads: A review. Const Build Mate 2020;237:117582. (10.1016/j.conbuildmat.2019.117582)

[24] Alhaidary H, Al–Tamimi AK. Importance of performance certification for post–installed anchors: an experimental assessment. Struct 2021;29:273–85. (10.1016/j.istruc.2020.11.005)

[25] ETAG 030, Guideline for European Technical Approval of Dowels for Structural Joints European Organization for Technical Approvals, Brussels, Belgium. 2013.

[26] Mahrenholtz C, Eligehausen R, Reinhardt H. Design of post–installed reinforcing bars as end anchorage or as bonded anchor. Eng Struct 2015;100:645–55. (10.1016/j.engstruct.2015.06.028)

[27] EOTA TR069, Design method for anchorage of post–installed reinforcing bars(rebars) with improved bond–splitting behavior as compared to EN 1992–1–1. European Organization for Technical Assessment, Brussels, Belgium. 2019.

[28] Maekawa K, Qureshi J. Stress transfer across interfaces in reinforced concrete due to aggregate interlock and dowel action, J Mater Struct Pavem 1997;557(V34):159–72. (10.2208/jscej.1997.557_159)

[29] Maekawa K, Fukura N, Soltani M. Path–dependent high cycle fatigue modeling of joint interfaces in structural concrete. J Advan Conc Tech 2008;6(1):227–42. (10.3151/jact.6.227)

[30] Xia J, Shan K, Wu X, Gan R, Jin W. Shear–friction behavior of concrete–to–concrete interface under direct shear load. Eng Struct 2021;238:112211. (10.1016/j.engstruct.2021.112211)

[31] Takase Y, Wada T, Ikeda T, Shinohara Y. Mechanical model of adhesive post–installed anchor subjected to cyclic shear force. Proc Frac Mech Concr. Concr Struct 2013:1727–36.

[32] Takase Y. Testing and modeling of dowel action for a post–installed anchor subjected to combined shear and tensile forces. Eng Strct 2019;195:551–8. (10.1016/j.engstruct.2019.05.086)

[33] Matsunaga K, Takase Y, Abe T. Modeling of dowel action for cast–in and post–installed anchors considering bond property. Eng Struct 2021;245:112773. (10.1016/j.engstruct.2021.112773)

[34] ACI 318–14. Building Code Requirements for Structural Concrete. American Concrete Institute, Farmington Hill, Michigan, 2014.

[35] AISC 360–16. Specifications for structural steel buildings. American Institute of Steel Construction, Chicago, Illinois, 2019

[36] Japanese Industrial Standards: JIS 1108, Method of test for compressive strength of concrete, 2018.

[37] Japanese Industrial Standards: JIS Z 2241, Metallic materials – Tensile testing – Method of test at room temperature, 2011.

[38] Eurocode 2. Design of concrete structures - Part 1-1: General rules and rules for building. European Committee for Standardization, Brussels, Belgium, 2004.